Free convection heat transfer of MgO-MWCNTs/EG hybrid nanofluid in a porous complex shaped cavity with MHD and thermal radiation effects

Received 19 April 2019
Revised 19 April 2019
Accepted 20 April 2019

Mohammad Ghalambaz
School of Aeronautic Science and Engineering, Beihang University, Beijing, PR China

Mahmoud Sabour
Young Researchers and Elite Club, Ahvaz Branch, Islamic Azad University, Ahvaz, Iran

Ioan Pop
Faculty of Mathematics and Computer Science, Babeş-Bolyai University, Cluj-Napoca, Romania, and

Dongsheng Wen
School of Aeronautic Science and Engineering, Beihang University, Beijing, China and School of Chemical and Process Engineering, University of Leeds, Leeds, UK

Abstract

Purpose – The present study aims to address the flow and heat transfer of MgO-MWCNTs/EG hybrid nanofluid in a complex shape enclosure filled with a porous medium. The enclosure is subject to a uniform inclined magnetic field and radiation effects. The effect of the presence of a variable magnetic field on the natural convection heat transfer of hybrid nanofluids in a complex shape cavity is studied for the first time. The geometry of the cavity is an annular space with an isothermal wavy outer cold wall. Two types of the porous medium, glass ball and aluminum metal foam, are adopted for the porous space. The governing equations for mass, momentum and heat transfer of the hybrid nanofluid are introduced and transformed into non-dimensional form. The actual available thermal conductivity and dynamic viscosity data for the hybrid nanofluid are directly used for thermophysical properties of the hybrid nanofluid.

Design/methodology/approach – The governing equations for mass, momentum and heat transfer of hybrid nanofluid are introduced and transformed into non-dimensional form. The thermal conductivity and dynamic viscosity of the nanofluid are directly used from the experimental results available in the literature. The finite element method is used to solve the governing equations. Grid check procedure and validations were performed.

This work of Mohammad Ghalambaz was supported by the STAR Institute – UBB, Cluj-Napoca, Romania, External Fellowship program, and the work by Ioan Pop has been supported from the Grant PN-III-P4-IDPCE-2016-0036, UEFISCDI, Romanian Ministry of Sciences.

The work was supported by National Science Foundation of China (No. 51876006), National Numerical Windtunnel (Grant 2018-ZT3A05) and 111 project (B18002). The authors wish also to express their thanks to the very competent Reviewers for the very good comments and suggestions.

International Journal of Numerical Methods for Heat & Fluid Flow
Vol. 29 No. 11, 2019
pp. 4349-4376

0961-5539
DOI 10.1108/HFF-04-2019-0339

Findings – The effect of Hartmann number, Rayleigh number, Darcy number, the shape of the cavity and the type of porous medium on the thermal performance of the cavity are studied. The outcomes show that using the composite nanoparticles boosts the convective heat transfer. However, the rise of the volume fraction of nanoparticles would reduce the overall enhancement. Considering a convective dominant regime of natural convection flow with Rayleigh number of 107, the maximum enhancement ratio (Nusselt number ratio compared to the pure fluid) for the case of glass ball is about 1.17 and for the case of aluminum metal foam is about 1.15 when the volume fraction of hybrid nanoparticles is minimum as 0.2 per cent.

Originality/value – The effect of the presence of a variable magnetic field on the natural convection heat transfer of a new type of hybrid nanofluids, MgO-MWCNTs/EG, in a complex shape cavity is studied for the first time. The results of this paper are new and original with many practical applications of hybrid nanofluids in the modern industry.

Keywords Porous media, Natural convection, Magnetohydrodynamic flow, MgO-MWCNTs/EG hybrid nanofluid

Paper type Research paper

Nomenclature

Latin symbols

B = Magnetic induction (flux density) (T);
C = Dimensional concentration of nanoparticles;
c_p = Specific heat at constant pressure ($JkgK^{-1}$);
Da = Darcy number;
$D_{l,s}$ = Large and small diameter;
g = Gravitational force (ms^{-2});
Ha = Hartmann number;
i = Number of grid points;
k = Thermal conductivity ($Wm^{-1}K^{-1}$), Dummy variable for numerical calculations;
L = Length of the enclosure (m);
N = Dummy variable for numerical calculations;
N_R = Radiation parameter;
Nu = Nusselt number;
P = Pressure (Pa);
Pr = Prandtl number;
R = Residual error;
Ra = Rayleigh number;
$R_{o,i,m}$ = Outer, inner and middle diameter;
$r_{o,i,m,s,l}$ = Outer, inner, middle, small and large radius (m);
T = Dimensional temperature (K);
u = Horizontal velocity along x-direction (ms^{-1});
v = Vertical velocity along y-direction (ms^{-1});
x = Cartesian coordinate x-direction (m); and
y = Cartesian coordinate y-direction (m).

Greek symbols

α = Thermal diffusivity (m^2s^{-1});
μ = Dynamic viscosity ($kgm^{-1}s^{-1}$);
β = Volumetric coefficient of thermal expansion (K);
γ = Penalty coefficient parameter;
θ = Dimensionless temperature;
ξ = Basis function;

ρ = Density (kgm^{-3}); and
σ = Electrical conductivity (sm^{-1}).

Subscripts
Avg = Average value;
bf = Base fluid;
C = Cold;
h = Hot;
hnf = Hybrid-Nanofluid;
ω = Angle of uniform magnetic field; and
0 = Reference.

Superscripts
* = Variables in dimensional form.

1. Introduction

The convective flow and heat transfer of an electrically conductive fluid in a magnetic field, magnetohydrodynamic (MHD) heat transfer, is of substantial attention in the recent metal-working and metallurgical applications. In MHD flows, the magnetic field can control the boundary-layer flow and heat transfer of an electrically conducting fluid. Some of the engineering applications of MHD flows are a nuclear reactor, MHD generators, plasma studies, purifications of metal from a non-metal mixture, geothermal energy extractions, metallurgy, polymer technology, the design of MHD power generators and MHD heat and mass transfer systems. Some of these applications can be found in the books by Cramer and Pai (1973), Branover and Tinober (1970), Shercliff (1965) and in the classical papers, for instance, Ingham (1973); Apelblat (1969); Liron and Wilhelm (1974); Goldsworthy (1961); Yih (1999) and Watanabe and Pop (1993).

Complex shape enclosures and wavy geometries are used in various engineering designs to enhance transport performance (Sheremet *et al.*, 2016). In this regard, many of literature studies addressed the natural convection heat transfer (Khanafer, 2014). For instance, Adjlout *et al.* (2002) theoretically addressed the influence of a wavy wall of the convective heat transfer for various value of Rayleigh number, cavity inclination angles. The outcomes reveal that the geometry of the cavity walls influences the flow and heat transfer rate in the cavity. Mahmud *et al.* (Free convection in an enclosure with vertical wavy walls, 2002) studied the effect of amplitude and aspect ratio of a wavy wall on the convective heat transfer characteristics in an enclosure. Yu and Xu (2018) investigated the effect of various thermal boundary conditions on the heat transfer in a cavity and revealed using a finite element method. The natural convection over vertical plates is also studied by Ahmed and Mahdy (2016) and Ahmed (2017).

Sheikholeslami *et al.* (2018) have presented the application of control volume finite element method (CVFEM) for the effect of magnetic field on nanofluid natural convection and radiation heat transfer through a porous medium using a non-Darcy model. Influences of Hartmann number, nanofluid volume fraction, Darcy number and Rayleigh number on thermal characteristics. Al-Najem *et al.* (1998) numerically investigated the impact of a transverse magnetic field on the laminar natural convection in a tilted enclosure. Mansour and El-Shaer (2002) studied the effect of magnetic field on non-Darcy axisymmetric free convection in a power-law fluid-saturated porous medium with variable permeability. Grosan *et al.* (2009) studied the effect of an internal heat generation source on the natural convection heat transfer in a rectangular enclosure subject to a magnetic field and filled with

a porous medium. Revnic *et al.* (2011) theoretically addressed the influence of a magnetic field on the unsteady natural convection heat transfer in a square cavity. The cavity was filled with a porous medium.

Javaherdeh and Najjarnezami (2018) investigated the magnetic field effects on the flow and heat transfer in a cavity filled with a porous medium. We also mention the paper by Sathiyamoorthy and Chamkha (2012) on natural convection flow under magnetic field in a square cavity for uniformly (or) linearly heated adjacent walls. Finally, we point out the review paper by Sheikholeslami and Rokni (2017) on the simulation of nanofluid heat transfer in the presence of a magnetic field. Doostani *et al.* (2017) and Ghalambaz *et al.* (2017a-2017d) addressed the natural convection and melting heat transfer of an MHD fluid in a cavity.

Invoking Rosseland approximation for thermal radiation, Magyari and Pantokratoras (2011) studied the effect of thermal radiation in the linearized Rosseland approximation on the heat transfer characteristics of various boundary layer flows. Martyushev and Sheremet (2012) have investigated the characteristics of Rosseland approximations in modeling nonstationary conditions of convection-radiation heat transfer in an enclosure with a local energy source. Also, Pop and Sheremet (2017) investigated the free convection in a square cavity filled with a Casson fluid under the effects of thermal radiation and viscous dissipation. Tahmasebi *et al.* (2018) and Mehryan *et al.* (2018) used the non-homogeneous Buongiorno's model to study the flow and heat transfer of nanofluids in a cavity with porous layers. Sheremet *et al.* (2018) addressed the natural convection flow and heat transfer of Al_2O_3-water nanofluid in a cavity filled with a porous medium.

After Huminic and Huminic (2018), hybrid nanofluids are a stable suspension of composite nanoparticles (with the size under 100 nm) utilized as a working fluid in heat transfer applications. Hybrid fluids contain two or three types of solid nanoparticles into a conventional fluid such as ethylene glycol, water or a mixture of water and ethylene glycol, kerosene, paraffin oil, vegetable oil or engine oil. Comprehensive reviews on nanofluids and hybrid nanofluids were presented by Mahian *et al.* (2018a, 2018b); Sarkar *et al.* (2015); Akilu *et al.*(2016); Sidik *et al.* (2016); Sundar *et al.* (2017) and Ranga Babu *et al.* (2017). We also mention here the papers by Mehryan *et al.* (2017, 2019), Ghalambaz *et al.* (2018); Hayat *et al.* (2018); Devi and Devi (2016) and Tayebi and Chamkha (2017) regarding the heat transfer of hybrid nanofluids. The phase change heat transfer of hybrid nanofluids was also addressed by Ghalambaz *et al.* (2017a-2017d); Chamkha *et al.* (2017) and Shao *et al.*, 2017.

Recently, MgO-MWCNT/Ethylene Glycol has been synthesized experimentally (Soltani and Akbari, 2016; Vafaei *et al.*, 2017). This nanofluid benefits from the high thermal conductive nanotubes and the MgO nanoparticles as an extra enhancer. The experimental data on the dynamic viscosity and thermal conductivity of the nanofluid are also available. Hence, this nanofluid is adopted for the theoretically study convective heat transfer in the present study.

The present study aims to analyze the effect of using MgO-MWCNT/Ethylene Glycol hybrid nanofluid on the natural convection flow and heat transfer a non-regular shape cavity filled with porous media subject to radiation and MHD effects.

2. Mathematical model and problem formulation

A non-regular shape porous cavity is studied in the present study. There is a hot tube in the center of the cavity and the outer walls of the cavity are wavy and cold. The space between the inner hot wall and the outer wavy cold walls is filled with a Darcy porous medium. Indeed, the outer wavy walls represent the smaller and cold pipes of a heat exchanger. The geometry of the cavity can be described in three steps as shown in Figure 1. Figure 2 shows the final geometry and used boundary conditions. In the present study, two types of the

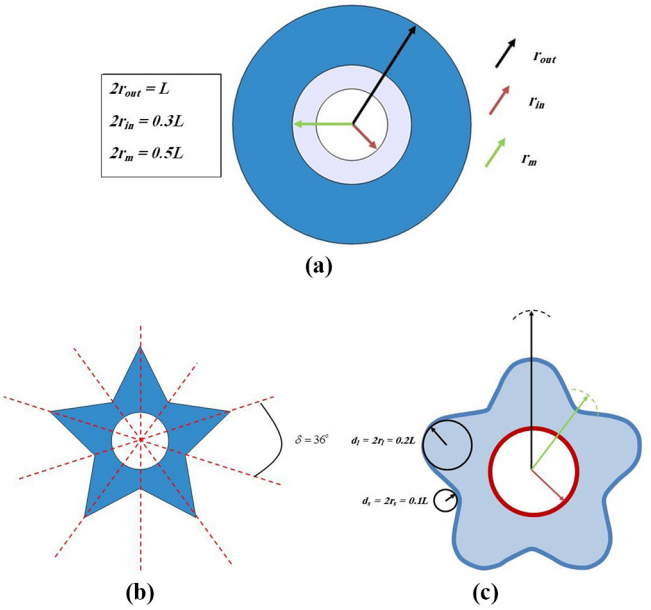

Notes: (a) The first step: inner, outer and a guided circle; (b) the second step: introducing star shape of the cavity using introduced circles; (c) the third step: introducing fillets at the edges

Figure 1.
The geometry shape of the cavity

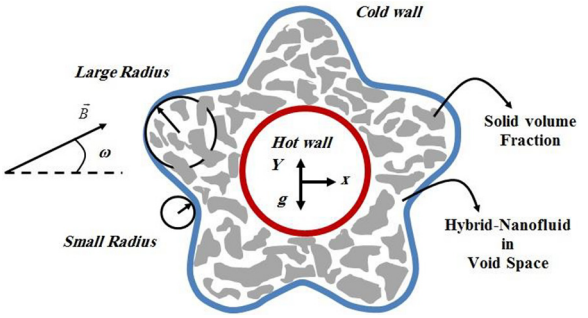

Figure 2.
Final schematic diagram of the physical model

porous medium, glass ball as a porous medium with low thermal conductivity and aluminum foam as a porous medium with very high thermal conductivity are adopted. The porous medium is saturated with MgO-MWCNT/EG hybrid nanofluid. The review of available literature regarding hybrid nanofluids shows that the regular or modified Brinkman and Maxwell models are not adequate for evaluating the dynamic viscosity and thermal conductivity of hybrid nanofluids (Mehryan *et al.*, 2019). Hence, in the present study, the actual experimental data of these type of hybrid nanofluids is used for calculations and will be discussed later.

The hybrid nanofluid is assumed as a stable homogeneous solution and it is assumed that the porous matrix is well treated to prevent interaction or sedimentation of nanoparticles with the porous structure. The hybrid nanofluid is a Newtonian incompressible and single-phase mixture of base fluid and nanoparticles. The thermophysical properties of the hybrid nanofluid are considered constant except the density, which is modeled using the Boussinesq approximation. Considering these assumptions, the Governing equations for conservation of mass, momentum and energy of the hybrid nanofluid are written as (Sheikholeslami *et al.*, 2018).

Hybrid-nanofluid continuity equation:

$$\frac{\partial u^*_{hnf}}{\partial x^*} + \frac{\partial v^*_{hnf}}{\partial y^*} = 0 \tag{1}$$

Momentum equations:

$$\frac{\rho_{hnf}}{\varepsilon^2}\left(u^*_{hnf}\frac{\partial u^*_{hnf}}{\partial x^*} + v^*_{hnf}\frac{\partial u^*_{hnf}}{\partial y^*}\right) = -\frac{\partial p^*}{\partial x^*} + \frac{\mu_{hnf}}{\varepsilon}\left(\frac{\partial^2 u^*_{hnf}}{\partial x^{*2}} + \frac{\partial^2 u^*_{hnf}}{\partial y^{*2}}\right)$$
$$-\frac{\mu_{hnf}}{K}u^*_{hnf} + \sigma_{hnf}B_0^2\left(v^*_{hnf}(\sin\omega)(\cos\omega) - u^*_{hnf}(\sin\omega)^2\right) \tag{2}$$

$$\frac{\rho_{hnf}}{\varepsilon^2}\left(u^*_{hnf}\frac{\partial v^*_{hnf}}{\partial x^*} + v^*_{hnf}\frac{\partial v^*_{hnf}}{\partial y^*}\right) = -\frac{\partial p^*}{\partial y^*} + \frac{\mu_{hnf}}{\varepsilon}\left(\frac{\partial^2 v^*_{hnf}}{\partial x^{*2}} + \frac{\partial^2 v^*_{hnf}}{\partial y^{*2}}\right)$$
$$-\frac{\mu_{hnf}}{K}v^*_{hnf} + \sigma_{hnf}B_0^2\left(u^*_{hnf}(\sin\omega)(\cos\omega) - v^*_{hnf}(\cos\omega)^2\right)$$
$$+\rho_{hnf}\beta_{hnf}(T - T_c)g \tag{3}$$

Thermal (energy) equation:

$$\left(u^*_{hnf}\frac{\partial T_{hnf}}{\partial x^*} + v^*_{hnf}\frac{\partial u^*_{hnf}}{\partial y^*}\right) = -\left(\frac{\partial q_r}{\partial x^*} + \frac{\partial q_r}{\partial y^*}\right) + \frac{k_{eff,hnf}}{(\rho c_p)_{hnf}}\left(\frac{\partial^2 T_{hnf}}{\partial x^{*2}} + \frac{\partial^2 T_{hnf}}{\partial y^{*2}}\right),$$
$$q_r = \frac{-4\sigma_e}{3\beta_R}\left(\frac{\partial T^4_{hnf}}{\partial x^*} + \frac{\partial T^4_{hnf}}{\partial y^*}\right)\frac{\partial T^4_{hnf}}{\partial y^*}, T^4_{hnf} \cong 4T_c T_{hnf} - 3T_c^4 \tag{4}$$

The corresponding boundary conditions for equations (1)-(4) are:

$$\begin{aligned} T_{hnf}.\vec{n} &= T_c \quad \text{for curved (outer) wall} \\ T_{hnf}.\vec{n} &= T_h \quad \text{for center (inner) wall} \\ u^*{}_{hnf}.\vec{n} &= v^*{}_{hnf} = 0 \quad \text{for all walls} \end{aligned} \tag{5}$$

where $\vec{n}$ is normal to the surface. The velocity at the walls is zero, which is the usual boundary condition for fluids next to a surface. It is assumed that the flow in the hot pipe and cold pipes is strong with high velocity. Hence, the convective heat transfer coefficient

inside the hot tube and inside the cold tubes is very high. Hence, the constant wall temperature is considered as the thermal boundary condition.

As mentioned MgO-MWCNT/EG is used as the working fluid. The thermal conductivity and dynamic viscosity of this hybrid nanofluid for the various concentration of hybrid nanoparticles are listed in Table I. In the present study, the nanofluid is consist of Ethylene Glycol and hybrid nanoparticles. The total volume fraction of nanoparticles is ϕ, which can be 0.2, 0.4 or 0.6 per cent. The volume fraction of ϕ is consist of MWCNT and MgO, which assumed to be equal. It should be noted that the total volume fraction of hybrid nanoparticles is very low as the hybrid nanofluids are synthesized with a low volume fraction of nanoparticles.

Due to the lack of appropriate models for accurate prediction of dynamic viscosity and thermal conductivity of hybrid nanofluids, the actual experimental data are directly incorporated in the covering equations. Indeed, the direct use of actual experimental data for thermal conductivity and dynamic viscosity of hybrid nanofluids bypasses the possible errors due to lack of appropriate physical models for thermophysical properties of hybrid nanofluids.

The effective thermal conductivity of the porous medium and hybrid nanofluid ($k_{eff,hnf}$) and the effective thermal conductivity of the porous medium and the base fluid ($k_{eff,bf}$) can be evaluated using the following relations (Nield and Bejan, 2017):

$$k_{eff,hnf} = (1-\varepsilon)k_{hnf} + \varepsilon k_s \tag{6}$$

$$k_{eff,bf} = (1-\varepsilon)k_{bf} + \varepsilon k_s \tag{7}$$

The density, ρ_{hnf} and heat capacity, $(\rho C_p)_{hnf}$, of the hybrid nanofluid, are obtained using (Ranga Babu *et al.*, 2017):

$$\rho_{hnf} = \phi_{mw}\rho_{mw} + \phi_p\rho_p + (1-\phi_{hnf})\rho_{bf} \tag{8}$$

$$(\rho C_p)_{hnf} = \phi_{mw}(\rho C_p)_{mw} + \phi_p(\rho C_p)_p + (1-\phi_{hnf})(\rho C_p)_{bf} \tag{9}$$

The volume coefficient of thermal expansion of the hybrid nanofluid, β_{hnf}, is calculated as:

$$\beta_{hnf} = \phi_{mw}\beta_{mw} + \phi_p\beta_p + (1-\phi_{hnf})\beta_{bf} \tag{10}$$

However, as the coefficient of thermal volume expansion of solids is one or two orders of magnitude smaller than that of liquids, β_{hnf} is approximated as $(1-\phi_{hnf})\beta_f$. Following the Maxwell model (Ranga Babu *et al.*, 2017), the electrical conductivity of the hybrid nanofluid is also evaluated as:

Table I. Determination of the dynamic viscosity ratio and thermal conductivity ratio as a function of temperature (°C) and volume fraction of nanoparticles (%), based on experimental data

ϕ_{hnf}	Thermal conductivity ratio k_{hnf}/k_{bf}	Dynamic viscosity ratio μ_{hnf}/μ_{bf}
0.2	1.11388	1.10346
0.4	1.15481	1.23450
0.6	1.19750	1.57070

Sources: Soltani and Akbari (2016); Vafaei *et al.* (2017)

$$\frac{\sigma_{hnf}}{\sigma_{bf}}=\frac{\frac{\left(\phi_{mw}\sigma_{mw}+\phi_{p}\sigma_{p}\right)}{\phi_{hnf}}+2\sigma_{bf}+2\left(\phi_{mw}\sigma_{mw}+\phi_{p}\sigma_{p}\right)-2\phi_{hnf}\sigma_{bf}}{\frac{\left(\phi_{mw}\sigma_{mw}+\phi_{p}\sigma_{p}\right)}{\phi_{hnf}}+2\sigma_{bf}-2\left(\phi_{mw}\sigma_{mw}+\phi_{p}\sigma_{p}\right)-2\phi_{hnf}\sigma_{bf}} \tag{11}$$

where indeed $(\phi_1\sigma_1+\phi_2\sigma_2)/\phi_{hnf}$ accounts for the effective electrical conductivity of hybrid particles. The electrical conductivity of some base fluids and nanoparticles has been reported in (Lewis and Wright, 1968; Sarojini *et al.*, 2013) as $\sigma_{EG}=10.7\times10^{-7}\ \mathrm{Sm}^{-1}$, $\sigma_{MgO}=5.392\times10^{-7}\ \mathrm{Sm}^{-1}$ and $\sigma_{MWCNT}=10\times10^{-15}\ \mathrm{Sm}^{-1}$.

Following (Ghalambaz *et al.*, 2015) two types of porous media are adopted in the present study, the aluminum foam as a high thermal conductive porous space and the glass ball as a low conductive porous space. The thermophysical properties of the nanoparticles and the porous media are summarized in Table II.

Now, the following non-dimensional parameters are used to transform the governing equations into a non-dimensional form:

$$\begin{aligned}
&x=\frac{x^*}{L}\ ,\ y=\frac{y^*}{L}\ ,\ u_{hnf}=\frac{u^*_{hnf}L}{\alpha_{eff,bf}}\ ,\ v_{hnf}=\frac{v^*_{hnf}L}{\alpha_{eff,bf}},\\
&p=\frac{p^*L^2}{\rho_{bf}\alpha^2_{eff,bf}},\ \theta_{hnf}=\frac{T_{hnf}-T_c}{T_h-T_c},\ R_i=\frac{2r_i}{L},\ R_o=\frac{2r_o}{L},\ R_m=\frac{2r_m}{L}\\
&D_l=\frac{2r_l}{L},\ D_s=\frac{2r_s}{L}.
\end{aligned} \tag{12}$$

Using equations (6), (7) and (12), the non- dimensional form of equations (1)-(4) are obtained as:

Continuity equation:

$$\frac{\partial u_{hnf}}{\partial x}+\frac{\partial v_{hnf}}{\partial y}=0 \tag{13}$$

Momentum equations in x and y directions:

$$\begin{aligned}
&\frac{1}{\varepsilon^2}\frac{\rho_{hnf}}{\rho_{bf}}\left(u_{hnf}\frac{\partial u_{hnf}}{\partial x}+v_{hnf}\frac{\partial u_{hnf}}{\partial y}\right)=-\frac{\partial p}{\partial x}+\frac{1}{\varepsilon}\frac{\mu_{hnf}}{\mu_{bf}}\mathrm{Pr}\left(\frac{\partial^2 u_{hnf}}{\partial x^2}+\frac{\partial^2 u_{hnf}}{\partial y^2}\right)-\frac{\mu_{hnf}}{\mu_{bf}}\frac{\mathrm{Pr}}{Da}u\\
&+\frac{\sigma_{hnf}}{\sigma_{bf}}Ha^2\mathrm{Pr}\left(v_{hnf}(\sin\omega)(\cos\omega)-u_{hnf}(\sin\omega)^2\right)
\end{aligned} \tag{14}$$

Table II. Thermophysical properties of the porous medium matrix, the nanoparticles and the base fluid

Property	Aluminum foam	Glass ball	MgO	MWCNT	Ethylene Glycol
C_p ($\mathrm{Jkg^{-1}K^{-1}}$)	897	840	879	711	2,415
k ($\mathrm{Wm^{-1}K^{-1}}$)	205	1.05	30	3,000	0.252
$\alpha\times10^{-7}$ ($\mathrm{m^2s^{-1}}$)	846.4	4.63	95.3	20,092.42	0.940
$\beta\times10^{-5}$ ($\mathrm{K^{-1}}$)	2.22	0.9	3.36	4.2	57
ρ ($\mathrm{kgm^{-3}}$)	2,700	2,700	3,580	2,100	1,110

Sources: Abu-Nada and Chamkha (2010); Afrand *et al.* (2017); Ghalambaz *et al.* (2015); Kalidasan and Kanna (2016)

$$\frac{1}{\varepsilon^2}\frac{\rho_{hnf}}{\rho_{bf}}\left(u_{hnf}\frac{\partial v_{hnf}}{\partial x}+v_{hnf}\frac{\partial v_{hnf}}{\partial y}\right)=-\frac{\partial p}{\partial y}+\frac{1}{\varepsilon}\frac{\mu_{hnf}}{\mu_{bf}}\Pr\left(\frac{\partial^2 v_{hnf}}{\partial x^2}+\frac{\partial^2 v_{hnf}}{\partial y^2}\right)-\frac{\mu_{hnf}}{\mu_{bf}}\frac{\Pr}{Da}v$$
$$+\frac{\sigma_{hnf}}{\sigma_{bf}}Ha^2\Pr\left(u_{hnf}(\sin\omega)(\cos\omega)-v_{hnf}(\cos\omega)^2\right)+\frac{\rho_{hnf}}{\rho_{bf}}\frac{\beta_{hnf}}{\beta_{bf}}Ra\Pr\theta \quad (15)$$

Thermal (energy) equation:

$$\left(u_{hnf}\frac{\partial\theta_{hnf}}{\partial x}+v_{hnf}\frac{\partial\theta_{hnf}}{\partial y}\right)=\left(\frac{4}{3}N_R+\frac{\alpha_{eff,hnf}}{\alpha_{eff,bf}}\right)\left(\frac{\partial^2\theta_{hnf}}{\partial x^2}+\frac{\partial^2\theta_{hnf}}{\partial y^2}\right) \quad (16)$$

Moreover, the non- dimensional form of boundary conditions are as below:

$$\begin{aligned}&\theta_{hnf}=0 \quad \text{for curved (outer) wall}\\&\theta_{hnf}=1 \quad \text{for center (inner) wall}\\&u_{hnf}=v_{hnf}=0 \quad \text{for all walls}\end{aligned} \quad (17)$$

The numbers and non- dimensional parameters are defined as:

$$\Pr=\frac{\mu_{bf}}{\rho_{bf}\alpha_{eff,bf}},\mathrm{Da}=\frac{K}{L^2},Ra=\frac{\rho_{bf}g\beta_{bf}(T_h-T_c)L^3}{\mu_{bf}\alpha_{eff,bf}},$$
$$Ha=LB_0\sqrt{\frac{\sigma_{bf}}{\mu_{bf}}},N_R=\frac{4\sigma_{SB}T_c^3}{a_R\alpha_{eff,bf}} \quad (18)$$

Effective Nusselt number as a criterion of heat transfer modes (conduction, convection and Radiation) for every point on the hot wall is:

$$Nu_l=-\left(\frac{k_{eff,hnf}}{k_{eff,bf}}+\frac{4}{3}N_R\right)\left(\frac{\partial\theta_{hnf}}{\partial n}\right)_{on\ hot\ wall} \quad (19)$$

And an average value of the non-dimensional Nusselt number is provided via:

$$Nu_{Avg}=-\frac{1}{2\pi R_{in}}\int_s Nu_l ds \quad (20)$$

Average Nusselt number Ratio is introduced as:

$$Nu_{ratio}=\frac{Nu_{Avg}}{Nu_{pure\ fluid(no-radiation,no-porous)}} \quad (21)$$

The average Nusselt number ratio shows the effect of the presence of porous media and radiation on the heat transfer rate in the cavity.

The average velocity in the cavity can be introduced as:

$$V_{Avg} = \frac{-\oiint V dA}{\oiint dA} \tag{22}$$

where A is the element area of the cavity and V is the velocity field defined as $V = (u_{hnf}^{2} + v_{hnf}^{2})^{1/2}$.

3. Numerical method and grid check and validation

3.1 Numerical method

The governing equations of equations (13)-(16) along with the boundary conditions of equation (17) are transformed into their weak form and then solved using the finite element method. A fully coupled Newton iteration method is used to integrate the equations. The iteration process continues until the residuals error for all variable be less than 10^{-6}. Details of the used finite element method are well described in the literature (Lewis *et al.*, 2004; Girault and Raviart, 2012; Reddy, 2018; Pepper, 2017).

The finite element method is used to solve the set of partial differential equations. As the continuity equation is a constraint for the velocity, a penalty approach is used to satisfy the continuity equation. Thus, the continuity equation is incorporated in the form of a penalty constraint for pressure in the momentum equations. So, the pressure term is introduced as:

$$P = -\gamma\left(\frac{\partial u_{hnf}}{\partial x} + \frac{\partial v_{hnf}}{\partial y}\right) \tag{23}$$

where γ is the penalty coefficient, which is a large number, $\gamma > 10^{+7}$. Substituting equation (24) for pressure term in momentum equations results in:

$$\frac{1}{\varepsilon^2}\frac{\rho_{hnf}}{\rho_{bf}}\left(u_{hnf}\frac{\partial u_{hnf}}{\partial x} + v_{hnf}\frac{\partial u_{hnf}}{\partial y}\right) = \gamma\frac{\partial}{\partial x}\left(\frac{\partial u_{hnf}}{\partial x} + \frac{\partial v_{hnf}}{\partial y}\right) + \frac{1}{\varepsilon}\frac{\mu_{hnf}}{\mu_{bf}}\Pr\left(\frac{\partial^2 u_{hnf}}{\partial x^2} + \frac{\partial^2 u_{hnf}}{\partial y^2}\right)$$
$$-\frac{\mu_{hnf}}{\mu_{bf}}\frac{\Pr}{Da}u_{hnf} + \frac{\sigma_{hnf}}{\sigma_{bf}}Ha^2\Pr\left(v_{hnf}(\sin\omega)(\cos\omega) - u_{hnf}(\sin\omega)^2\right) \tag{24}$$

$$\frac{1}{\varepsilon^2}\frac{\rho_{hnf}}{\rho_{bf}}\left(u_{hnf}\frac{\partial v_{hnf}}{\partial x} + v_{hnf}\frac{\partial v_{hnf}}{\partial y}\right) = \gamma\frac{\partial}{\partial y}\left(\frac{\partial u_{hnf}}{\partial x} + \frac{\partial v_{hnf}}{\partial y}\right) + \frac{1}{\varepsilon}\frac{\mu_{hnf}}{\mu_{bf}}\Pr\left(\frac{\partial^2 v_{hnf}}{\partial x^2} + \frac{\partial^2 v_{hnf}}{\partial y^2}\right)$$
$$-\frac{\mu_{hnf}}{\mu_{bf}}\frac{\Pr}{Da}v_{hnf} + \frac{\sigma_{hnf}}{\sigma_{bf}}Ha^2\Pr\left(u_{hnf}(\sin\omega)(\cos\omega) - v_{hnf}(\cos\omega)^2\right) + \frac{\beta_{hnf}}{\beta_{bf}}\frac{\rho_{hnf}}{\rho_{bf}}Ra\Pr\theta_{hnf} \tag{25}$$

By considering the large value of penalty coefficient γ, the continuity equation will be ensured. Now, the velocity components in x and y-direction and temperature are expanded using the basis of $\{\xi_k\}_{k=1}^{N}$ in the domain of solution:

$$u_{hnf} \approx \sum_{k=1}^{N} u_{hnf,k}\xi_k(x,y),\ v_{hnf} \approx \sum_{k=1}^{N} v_{hnf,k}\xi_k(x,y),\ \theta_{hnf} \approx \sum_{k=1}^{N} \theta_{hnf,k}\xi_k(x,y). \tag{26}$$

Now, by using the finite element method, the non-linear residuals for momentum in x and y directions and the energy equations are introduced as follows:

$$R_i^1 = \frac{1}{\varepsilon^2}\frac{\rho_{hnf}}{\rho_{bf}}\sum_{k=1}^{N} u_{hnf,k}\int_\Omega \left[\left(\sum_{k=1}^{N} u_{hnf,k}\xi_k(x,y)\right)\frac{\partial \xi_k}{\partial x} + \left(\sum_{k=1}^{N} v_{hnf,k}\xi_k(x,y)\right)\frac{\partial \xi_k}{\partial y}\right]\xi_i dxdy + \gamma$$
$$\left[\sum_{k=1}^{N} u_{hnf,k}\int_\Omega \frac{\partial \xi_i}{\partial x}\frac{\partial \xi_k}{\partial x} + \sum_{k=1}^{N} v_{hnf,k}\int_\Omega \frac{\partial \xi_i}{\partial x}\frac{\partial \xi_k}{\partial x}\right]dxdy + \frac{1}{\varepsilon}\frac{\mu_{hnf}}{\mu_{bf}}\mathrm{Pr}$$
$$\left[\sum_{k=1}^{N} v_{hnf,k}\int_\Omega \frac{\partial \xi_i}{\partial x}\frac{\partial \xi_k}{\partial x} + \frac{\partial \xi_i}{\partial y}\frac{\partial \xi_k}{\partial y}\right]dxdy - \frac{\mu_{hnf}}{\mu_{bf}}\frac{\mathrm{Pr}}{Da} + \int_\Omega \left(\sum_{k=1}^{N} u_{hnf,k}\xi_k(x,y)\right)\xi_i dxdy$$
$$\frac{\sigma_{hnf}}{\sigma_{bf}}Ha^2\mathrm{Pr}\left(\int_\Omega \left(\sum_{k=1}^{N} v_{hnf,k}\xi_k(x,y)\right)\xi_i dxdy(\sin\omega)(\cos\omega) - \int_\Omega \left(\sum_{k=1}^{N} u_{hnf,k}\xi_k(x,y)\right)\xi_i dxdy(\sin\omega)^2\right) \tag{27}$$

$$R_i^2 = \frac{1}{\varepsilon^2}\frac{\rho_{hnf}}{\rho_{bf}}\sum_{k=1}^{N} v_{hnf,k}\int_\Omega \left[\left(\sum_{k=1}^{N} u_{hnf,k}\xi_k(x,y)\right)\frac{\partial \xi_k}{\partial x} + \left(\sum_{k=1}^{N} v_{hnf,k}\xi_k(x,y)\right)\frac{\partial \xi_k}{\partial y}\right]\xi_i dxdy$$
$$+ \gamma\left[\sum_{k=1}^{N} u_{hnf,k}\int_\Omega \frac{\partial \xi_i}{\partial x}\frac{\xi_k}{\partial x} + \sum_{k=1}^{N} v_{hnf,k}\int_\Omega \frac{\partial \xi_i}{\partial y}\frac{\xi_k}{\partial y}\right]dxdy$$
$$+ \frac{1}{\varepsilon}\frac{\mu_{hnf}}{\mu_{bf}}\mathrm{Pr}\sum_{k=1}^{N} v_{hnf,k}\int_\Omega \left[\frac{\partial \xi_i}{\partial x}\frac{\xi_k}{\partial x} + \frac{\partial \xi_i}{\partial y}\frac{\xi_k}{\partial y}\right]dxdy - \frac{\mu_{hnf}}{\mu_{bf}}\frac{\mathrm{Pr}}{Da}\int_\Omega \left(\sum_{k=1}^{N} v_{hnf,k}\xi_k(x,y)\right)\xi_i dxdy$$
$$+ \frac{\sigma_{hnf}}{\sigma_{bf}}Ha^2\mathrm{Pr}\left(\int_\Omega \left(\sum_{k=1}^{N} u_{hnf,k}\xi_k(x,y)\right)\xi_i dxdy(\sin\omega)(\cos\omega) - \int_\Omega \left(\sum_{k=1}^{N} v_{hnf,k}\xi_k(x,y)\right)\xi_i dxdy(\cos\omega)^2\right)$$
$$+ \frac{\beta_{hnf}}{\beta_{bf}}\frac{\rho_{hnf}}{\rho_{bf}}Ra\mathrm{Pr}\int_\Omega \left(\sum_{k=1}^{N} \theta_{hnf,k}\xi_k(x,y)\right)\xi_i dxdy \tag{28}$$

$$R_i^3 = \frac{1}{\varepsilon}\sum_{k=1}^{N} \theta_{hnf,k}\int_\Omega \left[\left(\sum_{k=1}^{N} u_{hnf,k}\xi_k(x,y)\right)\frac{\partial \xi_k}{\partial x} + \left(\sum_{k=1}^{N} v_{hnf,k}\xi_k(x,y)\right)\frac{\partial \xi_k}{\partial y}\right]\xi_i dxdy$$
$$+ \left(\frac{4}{3}N_R + \frac{\alpha_{eff,hnf}}{\alpha_{eff,bf}}\right)\sum_{k=1}^{N} \theta_{hnf,k}\int_\Omega \left[\frac{\partial \xi_i}{\partial x}\frac{\xi_k}{\partial x} + \frac{\partial \xi_i}{\partial y}\frac{\xi_k}{\partial y}\right]dxdy \tag{29}$$

The integral terms in the above equation are calculated using three points Gaussian method. The two-point Gaussian method is used to calculate the related penalty terms. To minimize the residual, the calculations have been continued iteratively until the residual error of 10^{-6} achieved for all of the equations.

3.2 Grid check

In the present study, a non-uniform triangle mesh is used. Because of the importance of velocity and temperature gradients next to the cavity walls, a very fine grid is used to capture the important gradients properly. A view of the used grid consists of 151,218 meshes is depicted in Figure 3(a). The internal parts of the domain are meshed using triangular grids. Three magnified views of the used grid are depicted in Figures 3(b)-(d). To check the effect of the used grid on the accuracy of the solution, six different grid sizes are used. The results for the average Nusselt number and average fluid velocity are reported in Table III. As seen, as the Rayleigh number increases, a finer grid is required to maintain good accuracy. Based on the results of Table III, The grid size of 151,218 provides an accuracy sufficient for most of the engineering application. Hence, the results of the present study are reported for this gird size.

3.3 Validation

Four different configurations are used to validate the robustness and correctness of the present used solution procedure. As the first validation case, the results of the present study

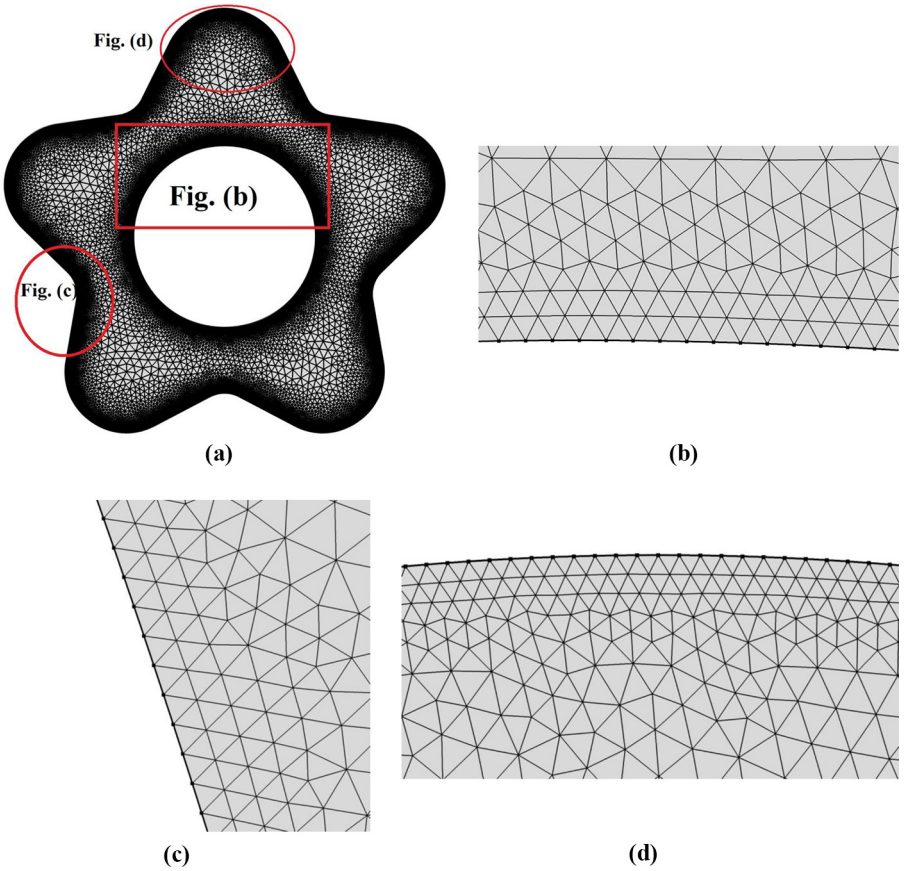

Figure 3.
Selected grid size for a star-shaped enclosure

are compared with those reported by Sathiyamoorthy and Chamkha (2012) for the case of MHD heat transfer in a square cavity. Assuming Darcy number as a very large value and considering zero volume fractions of nanoparticles ($\phi_{hnf} = 0$), the physic of the present study reduces to the study of Sathiyamoorthy and Chamkha (2012). Considering the geometry of a square cavity, $\omega = 0, N_R = 0, Ha = 100, \Pr = 0.054, Ra = 10^{+5}$, the temperature profiles obtained in the present study are compared with those reported by Sathiyamoorthy and Chamkha (2012). The outcomes are illustrated in Figure 4, which shows a very good agreement between the present results.

As the second validation, the temperature contours of this work are compared with the experimental outcomes of Guj *et al.* (1992) for the case of natural convection heat transfer in the space between two horizontal pipes when $\Pr = 0.7$, $Ra = 4.59 \times 10^4$ and other parameters as zero except the Darcy number, which is considered as a very large number. The results are depicted in Figure 5, which demonstrates a very good agreement with the present numerical solution and the experimental outcomes.

As the third validation case, the study of Sheremet and Pop (2015) is adopted. Sheremet and Pop (2015) addressed the natural convective heat transfer of nanofluids in a triangular cavity. The results for the average Nusselt number are compared in Figure 6.

Mesh size	Average Nusselt number $Ra = 10^{+5}$	$Ra = 10^{+6}$	$Ra = 10^{+7}$	Average velocity $Ra = 10^{+5}$	$Ra = 10^{+6}$	$Ra = 10^{+7}$
47,314	17.1451	18.4316	29.9890	3.1594	29.5434	177.9710
73,206	17.1442	18.4303	29.9842	3.1613	29.5614	178.0560
98,860	17.1441	18.4303	29.9821	3.1618	29.5669	178.0870
124,860	17.1436	18.4300	29.9798	3.1626	29.5728	178.0970
151,218	17.1434	18.4297	29.9789	3.1631	29.5789	178.1035
176,656	17.1434	18.4296	29.9793	3.1630	29.5770	178.0873

Notes: $\Pr = 155.261$, $N_R = 0.5$, $\varepsilon = 0.5$, $Da = 1$, $\phi = 0.4\%$, $\omega = 0^{\circ}$, $Ha = 10$, $R_o = 1$, $R_i = 0.3$, $R_m = 0.5$, $D_l = 0.2$ and $D_s = 0.1$ for glass ball

Table III.
Grid independency for average values of nusselt number and velocity in different values of rayleigh number

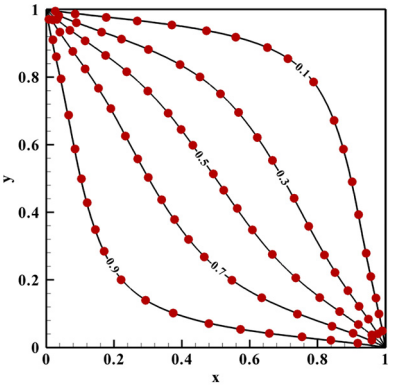

Notes: $\omega = 0$, $N_R = 0$, $\mathrm{Ha} = 100$, $\Pr = 0.054$, $\mathrm{Ra} = 10^{+5}$

Figure 4.
The non-dimensional temperature profiles in the cavity, present study (continuous lines) versus Sathiyamoorthy and Chamkha (2012a) marked by red points

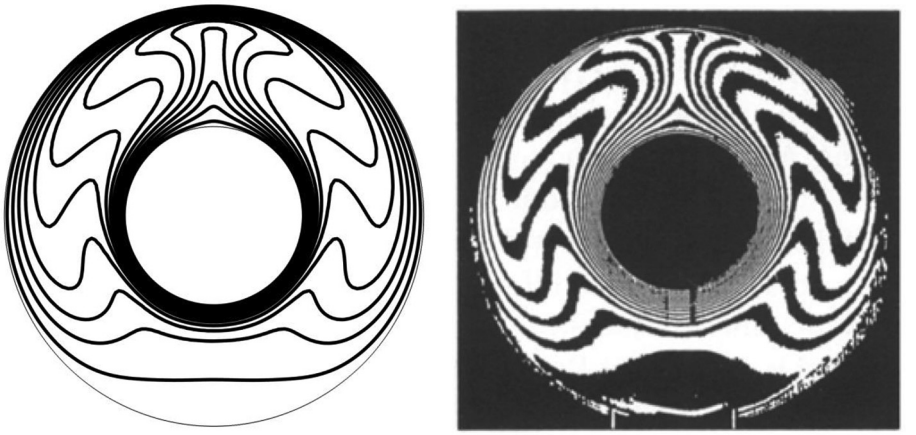

Figure 5.
Validation of isotherm contours

Sources: (a) Present work; (b) Guj *et al*. (1992)

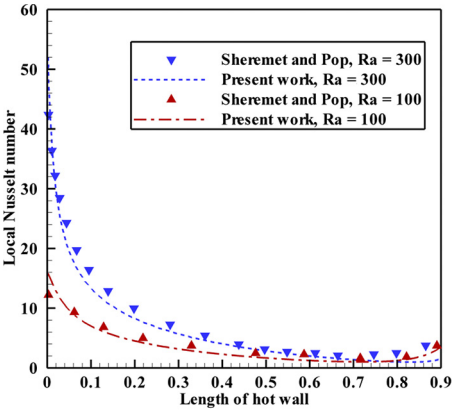

Figure 6.
Comparison of local Nusselt number between

Sources: (a) Present work; (b) Sheremet and Pop (2015)

The final validation case is for the natural convective heat transfer in a square cavity filled with a porous medium. The side wall of the cavity is subject to a temperature difference. Considering the very low value of Darcy number, the flow in the cavity can be reduced to the Darcy model and it would be independent of the value of the Prandtl number. Here, the value of Rayleigh (*Ra*) is indeed the Darcy-Rayleigh number or $Da \times Ra$. Considering the other parameters as zero, the average Nusselt number is evaluated and reported in Table IV. The results are compared with works of Baytas and Pop (1999); Sheremet and Pop (2014) and Ghalambaz *et al.* (2017a, 2017b, 2017c, 2017d). As seen, the outcomes of the present work are in agreement with the literature results.

4. Results and discussion

Following the literature works (Sheikholeslami *et al.*, 2018, Sheikholeslami and Rokni, 2017, Sathiyamoorthy and Chamkha, 2012), the range and the default values of the non-dimensional variables for the results of the present study are summarized in Table V. The Rayleigh number is considered a large value as in this study we are interested in convective heat transfer flows. The Prandtl number, outer diameter, inner diameter and middle diameter are fixed as Pr = 155.261, $R_o = 1$, $R_i = 0.3$, $R_m = 0.5$.

Figure 7 shows the isotherm contours and streamlines for a pure fluid with no magnetic field, radiation and nanoparticles. Indeed, the results of this figure can be considered as a basis for the study of more advanced cases including the radiation effects, magnetic field and hybrid nanofluids.

Figures 8 (a)-(d) show the local Nusselt number at the hot wall along the length of the wall in a counterclockwise direction. The results of this figure represent the local Nusselt number corresponding to those results of Figure 7. The average velocity and Nusselt number of each case have been reported in Figure 7. As seen in Figure 8, the maximum local heat transfer is at the bottom of the hot wall about $Nu_l = 38$ when $Ra = 10^7$. The minimum value of heat transfer is at the top of the hot wall about $Nu_l = 5.0$. Considering Figure 8, when the Rayleigh number is low, the isotherms show conduction-dominant regime in almost circular forms. By the increase of Rayleigh number, the natural convection flows get stronger and the convective dominant heat transfer can be observed. By the increase of Rayleigh number, the deflection of temperature curves increases and the temperature curves deflect to follow the fluid motion. Figures 8(c) and (d) show that the local Nusselt number gradually increases by moving along the hot wall from the bottom to top. Indeed, the fresh could fluid first reaches the bottom of the hot wall and this is where the heat transfer is maximum. After that, because of the interaction between the fluid and the hot wall, the fluids get hot and hotter and the temperature gradient between the fluid and the surface decreases, which as a results decreases the local Nusselt number. The streamlines of Figure 7(a) show that when the Rayleigh number is low, the convective flows are also weak; in this case, the streamlines precisely follow the cold wall shape. Figures 7(b) and (d) indicate

Table IV. Comparison between the Nusselt number values obtained in the presents study and those reported in the literature

Authors	*Ra* = 10	100	1,000	10,000
Baytas and Pop (1999)	1.079	3.160	14.060	48.330
Sheremet and Pop (2014)	1.071	3.104	13.839	49.253
Ghalambaz *et al.* (2017a, 2017b, 2017c, 2017d)	1.080	3.111	13.642	48.561
Present study	1.080	3.111	13.642	48.563

Table V. Default values of parameters and range of them

No.	Name of parameter	Default value	Lower bound	Upper bound
1	Rayleigh number (Ra)	10^6	10^5	10^7
2	Large diameter (D_l)	0.2	0	0.2
3	Small diameter (D_s)	0.1	0	0.1
4	Darcy number (Da)	1	10^{-4}	1
5	Porosity (ε)	0.5	0.1	0.9
6	Radiation parameter (N_R)	0.5	0.1	0.9
7	Hartmann number (Ha)	10	0	20
8	Volume faction of nanoparticles (ϕ)%	0.4	0.2	0.6

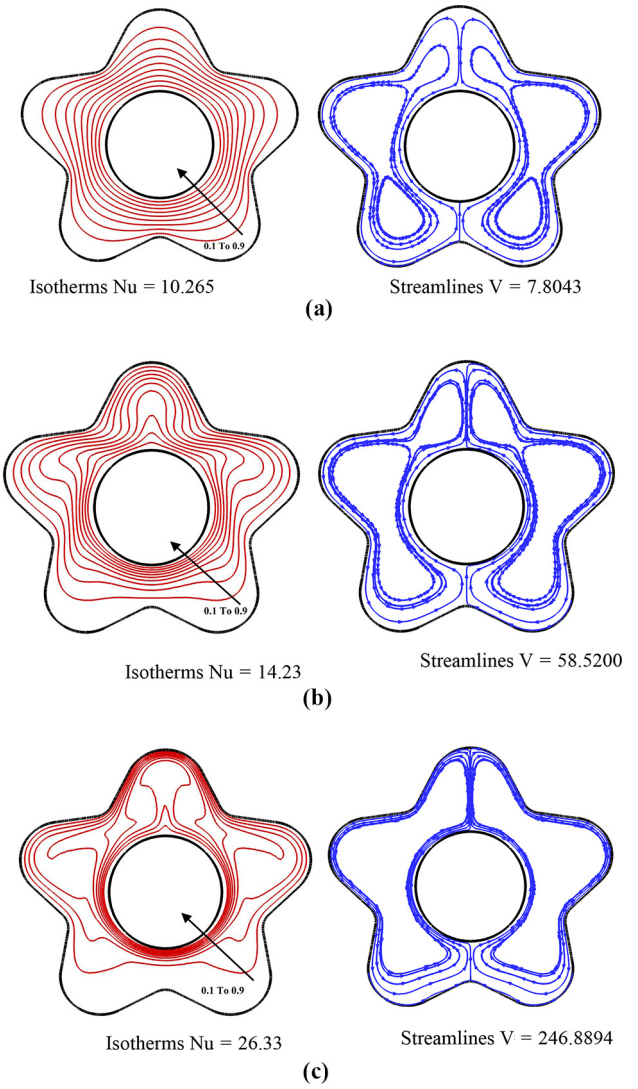

Figure 7.
Effect of Rayleigh number on the isotherms and streamlines for ethylene glycol pure fluid in simple media

Notes: Pr = 155.261, $N_R = 0$, $Ha = 0$, $\varepsilon = 0$, $R_o = 1$, $R_i = 0.3$, $R_m = 0.5$, $D_l = 0.2$ and $D_s = 0.1$). (a) $Ra = 10^5$; (b) $Ra = 10^6$; (c) $Ra = 10^7$

that the increase of Rayleigh number increases the streamlines next to the walls. So, the rise of *Ra* boosts the flow velocity in the cavity. The average velocity and Nusselt number gradually increase by the increase of *Ra*.

Figures 9 and 10 illustrate the isotherm and streamlines for two cases of glass ball porous space and aluminum foam, respectively. These figures represent the results for three

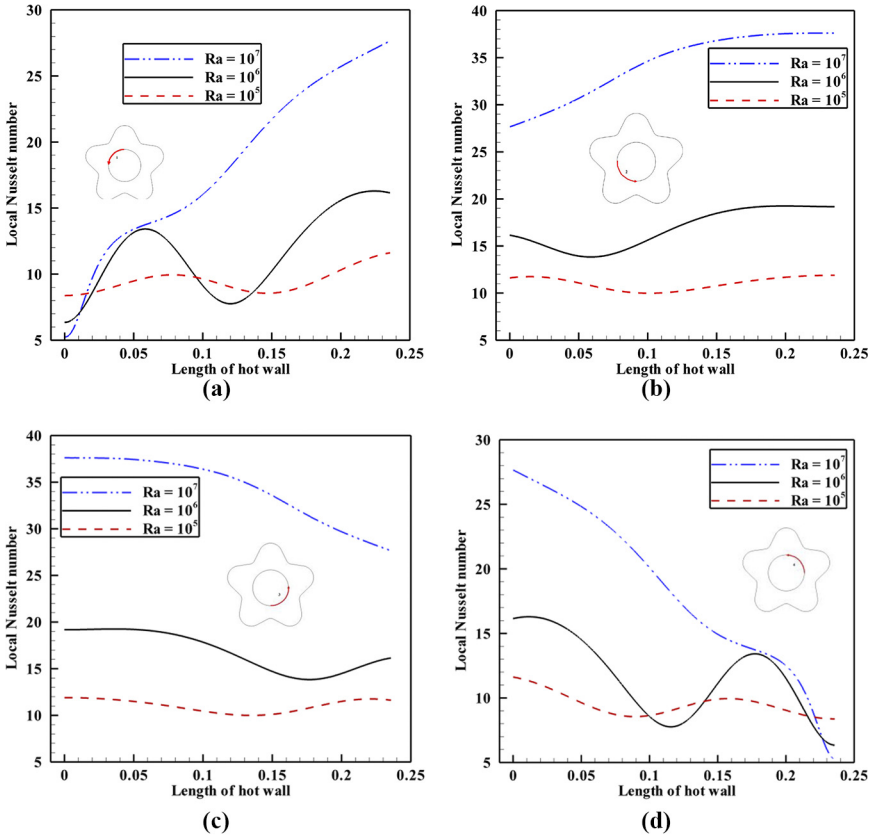

Figure 8.
Local Nusselt number on the hot wall (a) quarter 1; (b) quarter 2; (c) quarter 3 and (d) quarter 4, for ethylene glycol pure fluid in simple media

Notes: $Pr = 155.261$, $N_R = 0$, $H_a = 0$, $\varepsilon = 0$, $R_o = 1$, $R_i = 0.3$, $R_m = 0.5$, $D_l = 0.2$ and $D_s = 0.1$

different shapes of cavities. The corresponding local Nusselt number for the glass ball and aluminum foam are reported in Figures 11 and 12 adopting the cavity with the default shape and hybrid nanofluid volume fraction of 0.4 per cent.

Figures 9 and 10 show that changing the shape of the cavity walls can notably affect the isotherm and streamlines inside the cavity. Flattening the cavity edges reduces and increases the overall heat transfer rate and fluid velocity inside the cavity, respectively. Figures 11 and 12 show some picks in the local Nusselt number; these picks are because of the local circular fluid motions. Based on Figures 9 and 10, the average Nusselt number of the hybrid nanofluid for the case of glass ball porous space is higher than that of metal foam. However, Figures 11 and 12 reveal that the maximum local Nusselt number in the glass ball in lower than that of metal foam. The local Nusselt number changes following the shape of the outer cavity wall. When the cold wall is next to the hot wall the local Nusselt number increases. This is because of the fact that in these area the velocity of the flow is higher, and hence, the convection heat transfer is stronger.

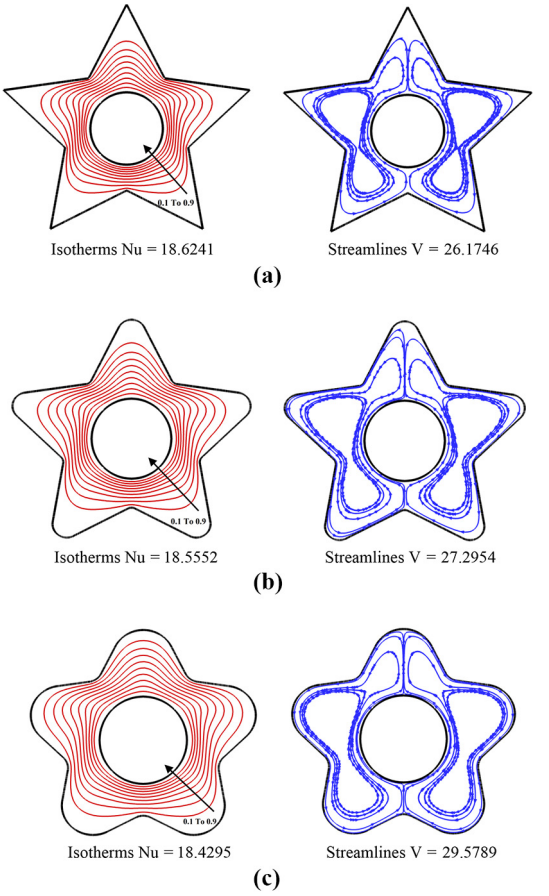

Figure 9.
Effect of cavity shape on the isotherms and streamlines

Notes: (a) $D_s = D_l = 0$; (b) $D_l = 0.1$, $D_s = 0.05$; (c) $D_l = 0.2$, $D_s = 0.1$ (D.V) for glass ball

Average Nusselt number is the important parameter of this study, which shows the overall heat transfer. Figures 13-16 are reported to study the average Nusselt number as a function of Darcy number, porosity, radiation parameter and Hartman number, respectively. The results are reported for various values of Rayleigh number and two cases of glass ball and aluminum foam porous medium. Figure 13 shows the influence of the Darcy number on the overall heat transfer rate in the cavity. As seen, the increase in *Da* increases the heat transfer rate. This effect is more obvious for a larger Rayleigh number, where there is a convective-dominant regime. Indeed, by raising of Darcy number the resistance of the media to flow motion reduces, and hence, the convective flows get strengthen.

Figure 14 shows the average Nusselt number as a function of porosity and for three values of Rayleigh number. When the Rayleigh number is small, $Ra = 10^5$, the increase of

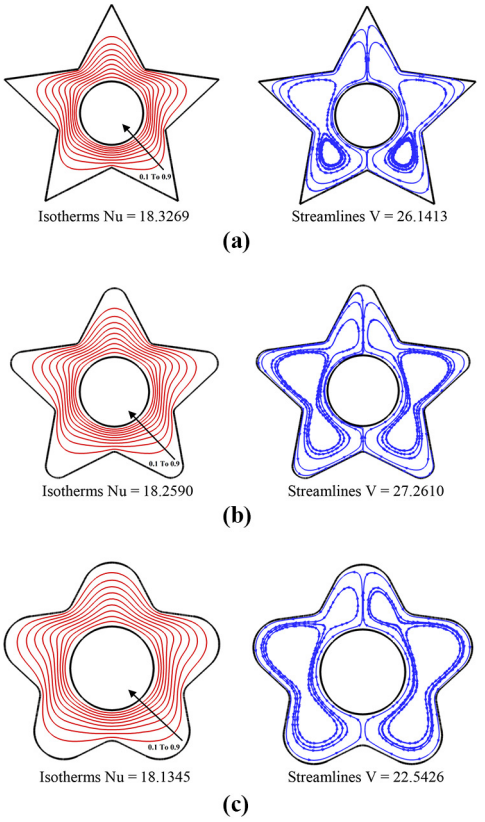

Notes: (a) $D_s = D_l = 0$; (b) $D_l = 0.1$, $D_s = 0.05$; (c) $D_l = 0.2$, $D_s = 0.1$ (D.V) for aluminum foam

Figure 10.
Effect of cavity shape on the isotherms and streamlines

porosity decreases the average Nusselt number. This is because in this case, the conduction effects are dominant and the increase of the porosity decreases the mass of the solid matrix. The thermal conductivity of the fluid is much lower that of the solid matrix. Hence, the rise of the porosity decreases the solid mass, which was contributed to the conduction mechanism, and hence, result in the decrease of the average Nusselt number. In contrast, when the Rayleigh number is high, the heat transfer is convective dominant, and hence, the increase of the porosity parameter increases the volume of the fluid and boosts the convective heat transfer. As a result, the rise of porosity raises the average Nusselt number. This outcome is almost the same for both cases of the glass ball and aluminum foam. The case of medium Rayleigh number, $Ra = 10^6$, shows a very small pick shape, which is the result of the two different effects those were discussed.

Figure 15 shows the average Nusselt number as a function of radiation parameter and four three values of Rayleigh number. The increase of radiation parameter N_R enhances the heat transfer. The effect of the Hartmann number on the heat transfer rate is studied in

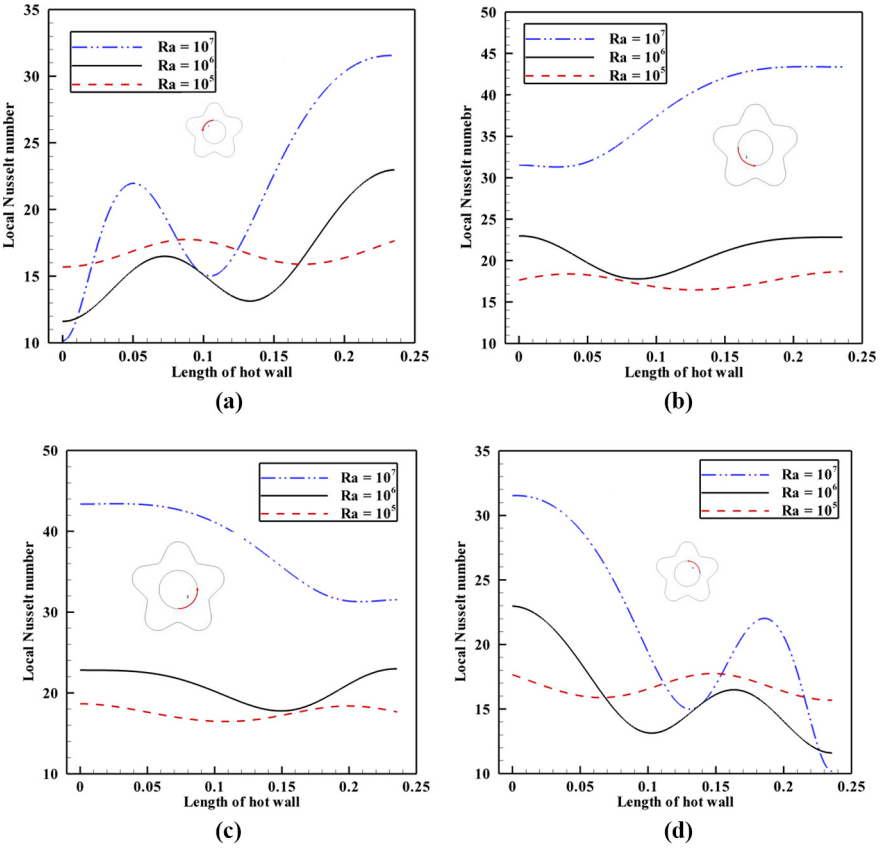

Figure 11.
Local Nusselt number on the hot wall

Notes: (a) Quarter 1; (b) quarter 2; (c) quarter 3; (d) quarter 4, for glass ball

Figure 16. This figure reveals that the augmentation of the magnetic field (*Ha*) slightly reduces the heat transfer rate. In the case of aluminum foam, the influence of the variation of *Ha* on the heat transfer is more obvious compared to that of the glass ball. The effect of the inclination angle of the magnetic field on the convective heat transfer was not significant, and hence, the results have not been plotted here.

Figure 17 is plotted to show the effect of volume fraction of hybrid nanoparticles on the heat transfer in the cavity. The results of this figure are plotted for the Nusselt number ratio as a function of the total volume fraction of hybrid nanoparticles. This figure compares the heat transfer because of the presence of nanoparticles with a reference case in which of the pure fluid with zero per cent of nanoparticles. As seen, the ratio of heat transfer of hybrid nanofluids to the base fluid is higher than unity, which shows enhancement of heat transfer by using hybrid nanoparticles in the overall chosen range for the volume fraction of nanoparticles. However, the increase of volume fraction of nanoparticles generally reduces the heat transfer rate. This figure interestingly reveals that using hybrid nanofluids in the glass ball porous space results in better thermal enhancement compared to that of the case of metal foam. Finally, this figure also shows that the increase in the overall concentration of

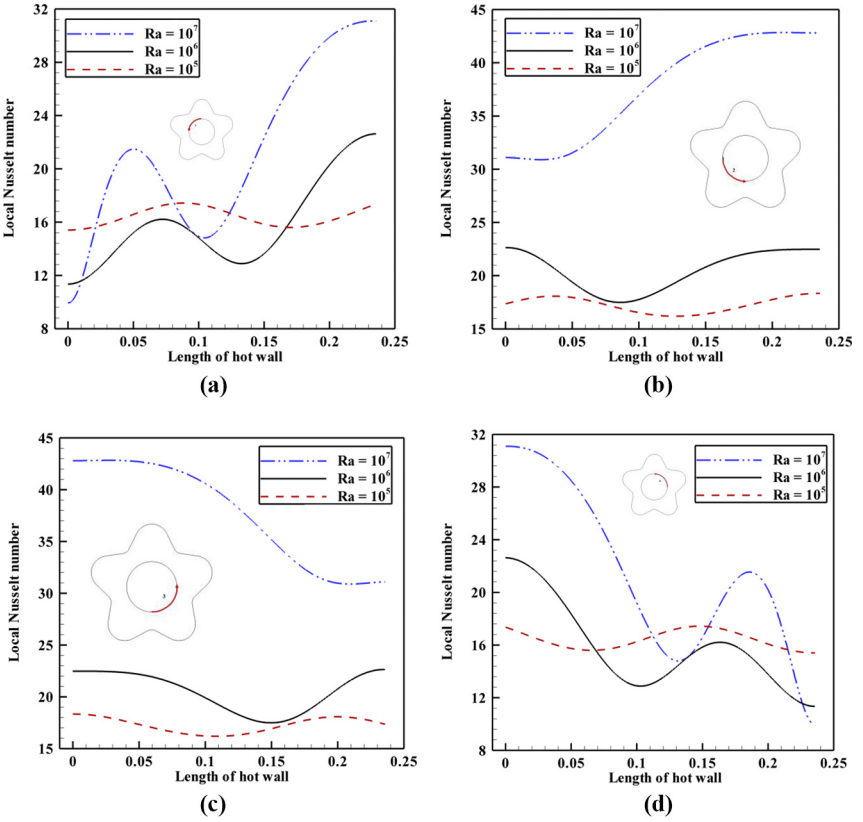

Notes: (a) Quarter 1; (b) quarter 2; (c) quarter 3; (d) quarter 4, for aluminum foam

Figure 12.
Local Nusselt number on the hot wall

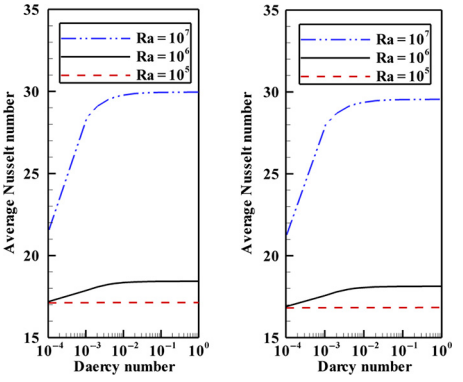

Figure 13.
Average Nusselt number as a function of Darcy number for glass ball (left side) and aluminum foam (right side) in various Rayleigh numbers

nanoparticles slightly improves the rate of heat transfer enhancement when the Rayleigh number is low, e.g. $Ra = 10^{+5}$. In fact, when Rayleigh number is low, the heat transfer is conduction-dominant, and hence, the increase of the volume fraction of nanoparticles enhances the thermal conductivity of the working fluid and consequently the heat transfer

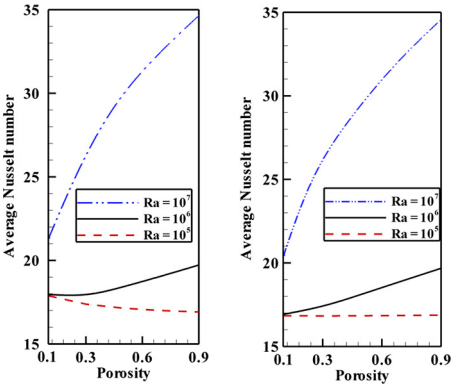

Figure 14.
Average Nusselt number as a function of porosity for glass ball (left side) and aluminum foam (right side) in various Rayleigh numbers

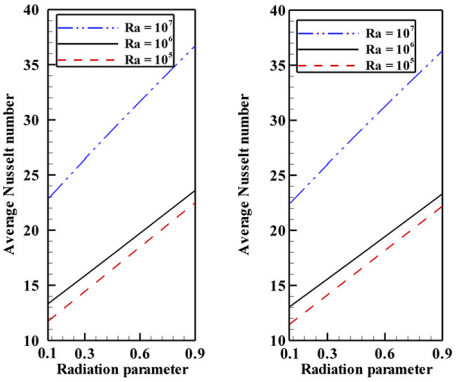

Figure 15.
Average Nusselt number as a function of radiation parameter for glass ball and aluminum foam (right side) in various Rayleigh numbers

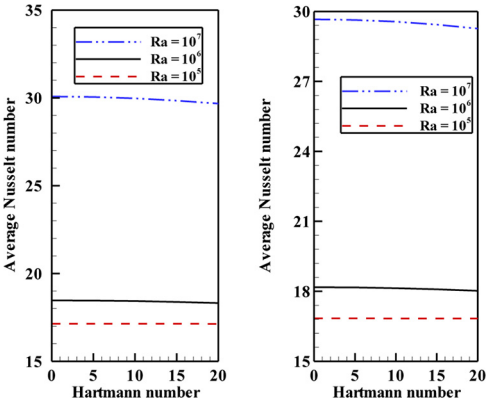

Figure 16.
Average Nusselt number as a function of Hartmann number for glass ball (left side) and aluminum foam (right side) in various Rayleigh numbers

rate in the enclosure. When the Rayleigh number is high (e.g. Rayleigh numbers, $Ra = 10^{+6}$ and $Ra = 10^{+7}$), using a higher concentration of nanoparticles results in the reduction of the heat transfer enhancement because of the rise of the dynamic viscosity.

5. Conclusions

The natural convection of a hybrid nanofluid, MgO-MWCNTs/EG, in a porous cavity is theoretically studied. The partial differential equations, representing the flow and heat transfer behavior of the hybrid nanofluid in the porous medium were introduced. Then, the governing equations were written in a non-dimensional form using non-dimensional variables to generalize the results. The obtained equations were integrated using the finite element method. Grid check and validation procedure were performed to ensure the accuracy of the results. The effect of the strength and inclination angle of the magnetic field, the type of porous medium, volume fraction of the composite nanoparticles and the porous-spaces characteristics such as Darcy number and porosity on the heat transfer in the cavity were addressed. The main outcomes of the present study can be summarized as follows:

- The geometry of the cavity induces minor effects on the flow and heat transfer patterns. A cavity with sharper edges results in a higher heat transfer rate.
- The increase of Rayleigh number, Darcy number and radiation parameter would increase the heat transfer rate in the cavity. The behavior of the porosity parameter depends on the magnitude of the Rayleigh number. For convective-dominant regimes, which Rayleigh number is high, the increase of the porosity would increase the heat transfer rate.
- The presence of hybrid nanoparticles enhances the heat transfer in the cavity. However, the increase of the concentration nanoparticles would reduce the magnitude of the enhancement. The maximum enhancement was observed for the very low volume fraction of nanoparticles, $\phi = 0.2$ per cent.
- The enhancement of using hybrid nanofluid is under the significant influence of the Rayleigh number. The Rayleigh number indeed indicates the regime of the fluid flow. Small values of the Rayleigh number represent a conduction-dominant heat transfer regime. The high values of Rayleigh number denote the convection heat transfer regime. The results of the present study show that when the Rayleigh number is low, $Ra = 10^5$, the enhancement ratio of using nanoparticles is very

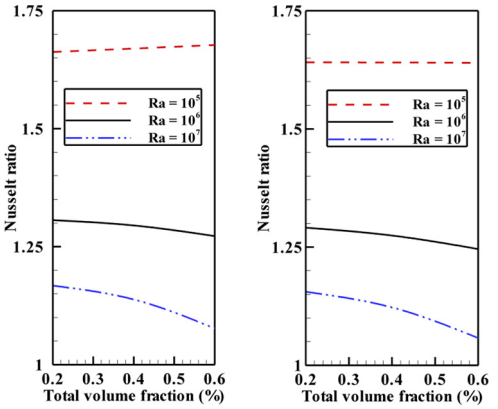

Figure 17. Nusselt ratio as a function of total volume fraction of nanoparticles for glass ball (left side) and aluminum foam (right side) in various Rayleigh numbers

significant about 1.65 at $\phi = 0.2$ per cent. However, as the Rayleigh number increases, the enhancement diminishes. In the case of $Ra = 10^7$, the enhancement ratio is about 1.15 at $\phi = 0.2$ per cent.

- The maximum enchantment ratio corresponds to the case of the porous medium glass ball with 1.17 at $\phi = 0.2$ per cent volume fraction of particles.
- The presence of the magnetic field smoothly reduces the heat transfer rate. The inclination angle of the magnetic field does not show a notable influence on the heat transfer performance of the hybrid nanofluid in the cavity.

References

Abu-Nada, E. and Chamkha, A.J. (2010), "Effect of nanofluid variable properties on natural convection in enclosures filled with a CuO–EG–water nanofluid", *International Journal of Thermal Sciences*, Vol. 49 No. 12, pp. 2339-2352.

Adjlout, L., Imine, O., Azzi, A. and Belkadi, M. (2002), "Laminar natural convection in an inclined cavity with a wavy wall", *International Journal of Heat and Mass Transfer, Pergamon*, Vol. 45 No. 10, pp. 2141-2152.

Afrand, M., Abedini, E. and Teimouri, H. (2017), "How the dispersion of magnesium oxide nanoparticles effects on the viscosity of water-ethylene glycol mixture: experimental evaluation and correlation development", *Physica E: Low-Dimensional Systems and Nanostructures*, Vol. 87, pp. 273-280.

Ahmed, S.E. (2017), "Modeling natural convection boundary layer flow of micropolar nanofluid over vertical permeable cone with variable wall temperature", *Applied Mathematics and Mechanics*, Vol. 38 No. 8, pp. 1171-1180.

Ahmed, S.E. and Mahdy, A. (2016), "Laminar MHD natural convection of nanofluid containing gyrotactic microorganisms over vertical wavy surface saturated non-Darcian porous media", *Applied Mathematics and Mechanics*, Vol. 37 No. 4, pp. 471-484.

Akilu, S., Sharma, K.V., Baheta, A.T. and Mamat, R. (2016), "A review of thermophysical properties of water based composite nanofluids", *Renewable and Sustainable Energy Reviews, Pergamon*, Vol. 66, pp. 654-678.

Al-Najem, N.M., Khanafer, K.M. and El-Refaee, M.M. (1998), "Numerical study of laminar natural convection in tilted enclosure with transverse magnetic field", *International Journal of Numerical Methods for Heat and Fluid Flow*, Vol. 8 No. 6, pp. 651-672.

Apelblat, A. (1969), "Application of the laplace transform to the solution of the boundary layer equations III: magnetohydrodynamic Falkner-Skan problem", *Journal of the Physical Society of Japan*, Vol. 27 No. 1, pp. 235-239.

Baytas, A.C. and Pop, I. (1999), "Free convection in oblique enclosures filled with a porous medium", *International Journal of Heat and Mass Transfer*, Vol. 42 No. 6, pp. 1047-1057.

Branover, G.G. and Tinober, A.B. (1970), *Magnetohydrodynamics of Incompressible Media (in Russian)*, Nauka, Moscow.

Chamkha, A.J., Doostanidezfuli, A., Izadpanahi, E. and Ghalambaz, M. (2017), "Phase-change heat transfer of single/hybrid nanoparticles-enhanced phase-change materials over a heated horizontal cylinder confined in a square cavity", *Advanced Powder Technology*, Vol. 28 No. 2, available at: https://doi.org/10.1016/j.apt.2016.10.009

Cramer, K.R. and Pai, S.I. (1973), *Magneto Fluid Dynamics for Engineers and Applied Physicists*, McGraw-Hill Book Company, Washington, DC.

Devi, S.S.U. and Devi, S.P.A. (2016), "Numerical investigation of three-dimensional hybrid Cu–Al_2O_3/water nanofluid flow over a stretching sheet with effecting Lorentz force subject to Newtonian heating", *Canadian Journal of Physics*, Vol. 94 No. 5, pp. 490-496.

Doostani, A., Ghalambaz, M. and Chamkha, A.J. (2017), "MHD natural convection phase-change heat transfer in a cavity: analysis of the magnetic field effect", *Journal of the Brazilian Society of Mechanical Sciences and Engineering*, Vol. 39 No. 7, available at: https://doi.org/10.1007/s40430-017-0722-z

Free convection in an enclosure with vertical wavy walls (2002), "Free convection in an enclosure with vertical wavy walls", *International Journal of Thermal Sciences*, Vol. 41 No. 5, pp. 440-446.

Ghalambaz, M., Sheremet, M.A. and Pop, I. (2015), "Free convection in a parallelogrammic porous cavity filled with a nanofluid using tiwari and das' nanofluid model", *PLoS ONE*, Vol. 10 No. 5, available at: https://doi.org/10.1371/journal.pone.0126486

Ghalambaz, M., Doostani, A., Chamkha, A.J. and Ismael, M.A. (2017a), "Melting of nanoparticles-enhanced phase-change materials in an enclosure: effect of hybrid nanoparticles", *International Journal of Mechanical Sciences*, Vol. 134, available at: https://doi.org/10.1016/j.ijmecsci.2017.09.045

Ghalambaz, M., Doostani, A., Izadpanahi, E. and Chamkha, A.J. (2017b), "Phase-change heat transfer in a cavity heated from below: the effect of utilizing single or hybrid nanoparticles as additives", *Journal of the Taiwan Institute of Chemical Engineers*, Vol. 72, available at: https://doi.org/10.1016/j.jtice.2017.01.010

Ghalambaz, M., Hendizadeh, H., Zargartalebi, H. and Pop, I. (2017c), "Free convection in a square cavity filled with a tridisperse porous medium", *Transport in Porous Media*, Vol. 116 No. 1, available at: https://doi.org/10.1007/s11242-016-0779-7

Ghalambaz, M., Doostanidezfuli, A., Zargartalebi, H. and Chamkha, A.J. (2017d), "MHD phase change heat transfer in an inclined enclosure: effect of a magnetic field and cavity inclination", *Numerical Heat Transfer; Part A: Applications*, Vol. 71 No. 1, available at: https://doi.org/10.1080/10407782.2016.1244397

Ghalambaz, M., Sheremet, M.A., Mehryan, S.A.M., Kashkooli, F.M. and Pop, I. (2018), "Local thermal non-equilibrium analysis of conjugate free convection within a porous enclosure occupied with Ag–MgO hybrid nanofluid", *Journal of Thermal Analysis and Calorimetry*, Vol. 135, pp. 1-18.

Girault, V. and Raviart, P.A. (2012), *Finite Element Methods for Navier-Stokes Equations: Theory and Algorithms*, Vol. 5, 1st ed., Springer-Verlag, Berlin Heidelberg, doi: 10.1007/978-3-642-61623-5.

Goldsworthy, F.A. (1961), "Magnetohydrodynamic flows of a perfectly conducting, viscous fluid", *Journal of Fluid Mechanics*, Vol. 11 No. 4, p. 519.

Grosan, T., Revnic, C., Pop, I. and Ingham, D.B. (2009), "Magnetic field and internal heat generation effects on the free convection in a rectangular cavity filled with a porous medium", *International Journal of Heat and Mass Transfer*, Vol. 52 Nos 5/6, pp. 1525-1533.

Guj, G., Iannetta, S. and Moretti, G. (1992), "Experimental analysis of thermal fields in horizontally eccentric cylindrical annuli", *Experiments in Fluids*, Vol. 12 No. 6, pp. 385-393.

Hayat, T., Nadeem, S. and Khan, A.U. (2018), "Rotating flow of Ag-CuO/H2O hybrid nanofluid with radiation and partial slip boundary effects", *The European Physical Journal E*, Vol. 41 No. 6, p. 75.

Huminic, G. and Huminic, A. (2018), "Hybrid nanofluids for heat transfer applications – a state-of-the-art review", *International Journal of Heat and Mass Transfer*, Vol. 125, pp. 82-103.

Ingham, D.B. (1973), "Impulsively started viscous flows past a finite flat plate with and without an applied magnetic field", *International Journal for Numerical Methods in Engineering*, Vol. 6 No. 4, pp. 521-527.

Javaherdeh, K. and Najjarnezami, A. (2018), "Lattice Boltzmann simulation of MHD natural convection in a cavity with porous media and sinusoidal temperature distribution", *Applied Mathematics and Mechanics*, Vol. 39 No. 8, pp. 1187-1200.

Kalidasan, K. and Kanna, P.R. (2016), "Effective utilization of MWCNT–water nanofluid for the enhancement of laminar natural convection inside the open square enclosure", *Journal of the Taiwan Institute of Chemical Engineers*, Vol. 65, pp. 331-340.

Khanafer, K. (2014), "Comparison of flow and heat transfer characteristics in a lid-driven cavity between flexible and modified geometry of a heated bottom wall", *International Journal of Heat and Mass Transfer*, Vol. 78, pp. 1032-1041.

Lewis, R.W., Nithiarasu, P. and Seetharamu, K.N. (2004), *Fundamentals of the Finite Element Method for Heat and Fluid Flow*, John Wiley & Sons.

Lewis, T.J. and Wright, A.J. (1968), "The electrical conductivity of magnesium oxide at low temperatures", *Journal of Physics D: Applied Physics*, Vol. 1 No. 4, p. 305.

Liron, N. and Wilhelm, H.E. (1974), "Integration of the magnetohydrodynamic Boundary-Layer equations by meksyn's method", *ZAMM – Zeitschrift Für Angewandte Mathematik Und Mechanik*, Vol. 54 No. 1, pp. 27-37.

Magyari, E. and Pantokratoras, A. (2011), "Note on the effect of thermal radiation in the linearized rosseland approximation on the heat transfer characteristics of various boundary layer flows", *International Communications in Heat and Mass Transfer*, Vol. 38 No. 5, pp. 554-556.

Mahian, O., Kolsi, L., Amani, M., Estellé, P., Ahmadi, G., Kleinstreuer, C., Marshall, J.S., Siavashi, M., Taylor, R.A., Niazmand, H., Wongwises, S., Hayat, T., Kolanjiyil, A., Kasaeian, A. and Pop, I. (2018a), "Recent advances in modeling and simulation of nanofluid flows-part I: fundamental and theory", *Physics Reports*, Vol. 790.

Mahian, O., Kolsi, L., Amani, M., Estellé, P., Ahmadi, G., Kleinstreuer, C., Marshall, J.S., Siavashi, M., Taylor, R.A., Niazmand, H., Wongwises, S., Hayat, T., Kolanjiyil, A., Kasaeian, A. and Pop, I. (2018b), "Recent advances in modeling and simulation of nanofluid flows-part II: applications", *Physics Reports*, Vol. 791.

Mansour, M.A. and El-Shaer, N.A. (2002), "Effect of magnetic field on non-Darcy axisymmetric free convection in a power-law fluid saturated porous medium with variable permeability", *Journal of Magnetism and Magnetic Materials*, Vol. 250, pp. 57-64.

Martyushev, S.G. and Sheremet, M.A. (2012), "Characteristics of rosseland and P-1 approximations in modeling nonstationary conditions of convection-radiation heat transfer in an enclosure with a local energy source", *Journal of Engineering Thermophysics*, Vol. 21 No. 2, pp. 111-118.

Mehryan, S.A.M., Ghalambaz, M. and Izadi, M. (2018), "Conjugate natural convection of nanofluids inside an enclosure filled by three layers of solid, porous medium and free nanofluid using buongiorno's and local thermal non-equilibrium models", *Journal of Thermal Analysis and Calorimetry*, Vol. 1, pp. 1-21.

Mehryan, S.A.M., Kashkooli, F.M., Ghalambaz, M. and Chamkha, A.J. (2017), "Free convection of hybrid Al2O3-Cu water nanofluid in a differentially heated porous cavity", *Advanced Powder Technology*, Vol. 28 No. 9, available at: https://doi.org/10.1016/j.apt.2017.06.011

Mehryan, S.A.M., Izadpanahi, E., Ghalambaz, M. and Chamkha, A.J. (2019), "Mixed convection flow caused by an oscillating cylinder in a square cavity filled with Cu–Al_2O_3/water hybrid nanofluid", *Journal of Thermal Analysis and Calorimetry*, Vol. 1, pp. 1-18, available at: https://doi.org/10.1007/s10973-019-08012-2

Nield, D.A. and Bejan, A. (2017), "Heat transfer through a porous medium", *Convection in Porous Media*, Springer International Publishing, Cham, pp. 37-55.

Pepper, D. (2017), *The Intermediate Finite Element Method: Fluid Flow and Heat Transfer Applications*, Routledge.

Pop, I. and Sheremet, M. (2017), "Free convection in a square cavity filled with a casson fluid under the effects of thermal radiation and viscous dissipation", *International Journal of Numerical Methods for Heat and Fluid Flow*, Vol. 27 No. 10, pp. 2318-2332.

Ranga Babu, J.A., Kumar, K.K. and Srinivasa Rao, S. (2017), "State-of-art review on hybrid nanofluids", *Renewable and Sustainable Energy Reviews*, Vol. 77, pp. 551-565.

Reddy, J.N. (2018), *Introduction to the Finite Element Method*, 4th ed., McGraw-Hill Education, New York.

Revnic, C., Grosan, T., Pop, I. and Ingham, D.B. (2011), "Magnetic field effect on the unsteady free convection flow in a square cavity filled with a porous medium with a constant heat generation", *International Journal of Heat and Mass Transfer*, Vol. 54 Nos 9/10, pp. 1734-1742.

Sarkar, J., Ghosh, P. and Adil, A. (2015), "A review on hybrid nanofluids: recent research, development and applications", *Renewable and Sustainable Energy Reviews*, Vol. 43, pp. 164-177.

Sarojini, K.G.K., Manoj, S.V., Singh, P.K., Pradeep, T. and Das, S.K. (2013), "Electrical conductivity of ceramic and metallic nanofluids", *Colloids and Surfaces A: Physicochemical and Engineering Aspects*, Vol. 417, pp. 39-46.

Sathiyamoorthy, M. and Chamkha, A.J. (2012), "Natural convection flow under magnetic field in a square cavity for uniformly (or) linearly heated adjacent walls", *International Journal of Numerical Methods for Heat and Fluid Flow*, Vol. 22 No. 5, pp. 677-698.

Shao, X.-F., Mo, S.-P., Chen, Y., Yin, T., Yang, Z., Jia, L.-S. and Cheng, Z.-D. (2017), "Solidification behavior of hybrid TiO_2 nanofluids containing nanotubes and nanoplatelets for cold thermal energy storage", *Applied Thermal Engineering*, Vol. 117, pp. 427-436.

Sheikholeslami, M. and Rokni, H.B. (2017), "Simulation of nanofluid heat transfer in presence of magnetic field: a review", *International Journal of Heat and Mass Transfer*, Vol. 115, pp. 1203-1233.

Sheikholeslami, M., Li, Z. and Shamlooei, M. (2018), "Nanofluid MHD natural convection through a porous complex shaped cavity considering thermal radiation", *Physics Letters A*, Vol. 382 No. 24, pp. 1615-1632.

Shercliff, J.A. (1965), *A Textbook of Magnetohydrodynamics*, Pergamon Press, Oxford, New York, NY.

Sheremet, M.A. and Pop, I. (2014), "Natural convection in a square porous cavity with sinusoidal temperature distributions on both side walls filled with a nanofluid: Buongiorno's mathematical model", *Transport in Porous Media*, Vol. 105 No. 2, pp. 411-429.

Sheremet, M.A. and Pop, I. (2015), "Free convection in a triangular cavity filled with a porous medium saturated by a nanofluid: Buongiorno's mathematical model", *International Journal of Numerical Methods for Heat and Fluid Flow*, Vol. 25 No. 5, pp. 1138-1161.

Sheremet, M.A., Pop, I. and Roşca, N.C. (2016), "Magnetic field effect on the unsteady natural convection in a wavy-walled cavity filled with a nanofluid: Buongiorno's mathematical model", *Journal of the Taiwan Institute of Chemical Engineers*, Vol. 61, pp. 211-222.

Sheremet, M., Trîmbiţaş, R., Groşan, T. and Pop, I. (2018), "Natural convection of an alumina-water nanofluid inside an inclined wavy-walled cavity with a non-uniform heating using tiwari and das' nanofluid model", *Applied Mathematics and Mechanics*, Vol. 30 No. 10, pp. 1425-1436.

Sidik, N.A.C., Adamu, I.M., Jamil, M.M., Kefayati, G.H.R., Mamat, R. and Najafi, G. (2016), "Recent progress on hybrid nanofluids in heat transfer applications: a comprehensive review", *International Communications in Heat and Mass Transfer*, Vol. 78, pp. 68-79.

Soltani, O. and Akbari, M. (2016), "Effects of temperature and particles concentration on the dynamic viscosity of MgO-MWCNT/ethylene glycol hybrid nanofluid: experimental study", *Physica E: Low-Dimensional Systems and Nanostructures*, Vol. 84, pp. 564-570.

Sundar, L.S., Sharma, K.V., Singh, M.K. and Sousa, A.C.M. (2017), "Hybrid nanofluids preparation, thermal properties, heat transfer and friction factor – a review", *Renewable and Sustainable Energy Reviews*, Vol. 68, pp. 185-198.

Tahmasebi, A., Mahdavi, M. and Ghalambaz, M. (2018), "Local thermal nonequilibrium conjugate natural convection heat transfer of nanofluids in a cavity partially filled with porous media

using buongiorno's model", *Numerical Heat Transfer, Part A: Applications*, Vol. 73 No. 4, pp. 254-276.

Tayebi, T. and Chamkha, A.J. (2017), "Buoyancy-driven heat transfer enhancement in a sinusoidally heated enclosure utilizing hybrid nanofluid", *Computational Thermal Sciences: An International Journal*, Vol. 9 No. 5, pp. 405-421.

Vafaei, M., Afrand, M., Sina, N., Kalbasi, R., Sourani, F. and Teimouri, H. (2017), "Evaluation of thermal conductivity of MgO-MWCNTs/EG hybrid nanofluids based on experimental data by selecting optimal artificial neural networks", *Physica E: Low-Dimensional Systems and Nanostructures*, Vol. 85, pp. 90-96.

Watanabe, T. and Pop, I. (1993), "Magnetohydrodynamic free convection flow over a wedge in the presence of a transverse magnetic field", *International Communications in Heat and Mass Transfer*, Vol. 20 No. 6, pp. 871-881.

Yih, K.A. (1999), "MHD forced convection flow adjacent to a non-isothermal wedge", *International Communications in Heat and Mass Transfer*, Vol. 26 No. 6, pp. 819-827.

Yu, Q. and Xu, H. (2018), "Novel wavelet-homotopy galerkin technique for analysis of lid-driven cavity flow and heat transfer with non-uniform boundary conditions", *Applied Mathematics and Mechanics*, Vol. 39 No. 12, pp. 1691-1718.

Corresponding authors
Mohammad Ghalambaz can be contacted at: m.ghalambaz@gmail.com; m.ghalambaz@iaud.ac.ir and Donghsheng Wen can be contacted at: d.wen@buaa.edu.cn; d.wen@leeds.ac.uk